Core-scale characterization of hydraulic and poroelastic properties using oscillating pore pressure method

Azar K. Hasanov [1], Brandon Dugan [2] and Michael L. Batzle[2†]

[1] Shell Exploration and Production Company, Houston, USA [2] Department of Geophysics, Colorado School of Mines, Golden, USA [†] Deceased on 9 January 2015

INTRODUCTION

Knowledge of hydraulic and poroelastic properties is essential for simulating fluid flow in porous media. Accurate constraints on these properties have impacts on production forecasts and economics. In this study we document an improvement of the oscillating pore pressure experiment by simultaneously measuring hydraulic and poroelastic properties of reservoir rocks. Measurements were carried out on four conventional reservoir rock quality samples at oscillation frequencies of 0.025-1 Hz and effective pressures of 3.5-62 MPa. Estimated permeability values decreased with increasing effective pressure and increased sharply above a frequency range of 0.3-0.4 Hz. We established that hydraulically measured storage capacities are overestimated by almost an order of magnitude when compared to elastically derived ones. Biot coefficient was estimated both from hydraulic and strain measurements, and comparison of two data sets reveals high uncertainty of the hydraulic specific storage measurements. We documented grain crushing and pore collapse event in a dolostone sample, observed as a permanent and drastic decrease of permeability and bulk modulus. We validated our method by detecting irreversible microstructural changes independently by hydraulic, elastic, X-ray microtomography (μCT) and nuclear magnetic resonance (NMR) measurements. Our approach can be used to constrain and to improve the estimation of specific storage and thus leads to better model inputs and forecasts.

We develop a novel data processing approach that utilizes a broad, multifrequency range of data and inverts it for permeability. We re-process published data and demonstrate that our methodology outperforms traditional data reduction techniques, as our inversion results show a better fit to pressure trends. To better understand the effect of frequency on phase and amplitude data and to verify our inversion approach we numerically simulate oscillating pore pressure experiments for four rock samples. We document a strong deviation of experimentally obtained phase data starting at 0.3 Hz oscillation frequency. A possible explanation for this deviation is deformation coupling during pressure diffusion. Our method can be used for robust determination of permeability and rapid prediction of experimental results using numerical simulation, ultimately improving the analysis of experimental permeability measurements.

Permeability and storage capacities are calculated using Kranz et al. (1992) or Adachi & Detournay (1997) method. These models are based on an analytical solution of 1-D diffusion equation with oscillatory boundary conditions. The downstream-to-upstream pressure amplitude ratio (R) and phase lag (θ) are functions of these rock properties and sample characteristics:

$$Re^{-i\theta} = \frac{1+\frac{B}{3}\left[\cosh\left(\lambda(1+i)\right)-1\right]}{\frac{\lambda}{\psi}(1+i)\sinh\left(\lambda(1+i)\right)+\cosh\left(\lambda(1+i)\right)}$$

MOTIVATION - AQUIFER CHARACTERIZATION

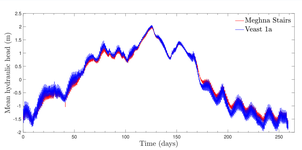

Figure 1: Hydraulic head measured in shallow aquifer boreholes near Meghna river, Bangladesh (from Sobolevskaia et al. (2019, in preparation)).

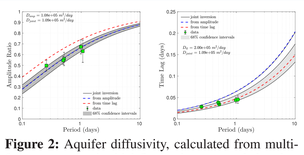

Figure 2: Aquifer diffusivity, calculated from multi-frequency oceanic tidal fluctuations, recorded as hydraulic head time-series (from Sobolevskaia et al. (2019, in preparation)).

SAMPLES

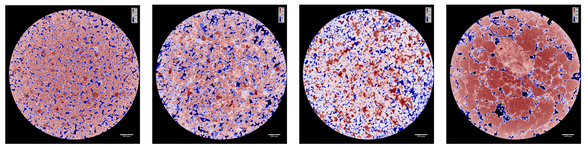

(a) Navajo 7 sandstone (b) Fox Hills 7 sandstone (c) Berea 2 sandstone (d) San-Andres 1 dolostone

Figure 3: μCT-scans of the studied samples.

Table 1: Dimensions and petrophysical properties of the studied samples.

	Samples			
	Navajo 7	Fox Hills 7	Berea 2	San-Andres 1
Length (mm)	110	120.7	103.7	134.8
Porosity (%)	19.94	27.12	15.65	17.29
Gas permeability (mD)	74	62	110	165
Grain density (g/cm^3)	2.55	2.58	2.61	2.83
Mineral bulk modulus (GPa)	31.67	20.93	34.33	89.20

EXPERIMENTAL METHODOLOGY

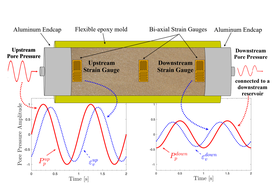

Figure 4: A generic schematic of the oscillating pore pressure experiment. A controlled upstream pore pressure sinusoid propagates through a porous sample and is recorded at the downstream face of the sample. The downstream sinusoid has a diminished amplitude and a phase lag. The same amplitude and phase behaviors apply to the volumetric strain signals. The pore pressure and the generated volumetric strain are out-of-phase because the measurements are not co-located.

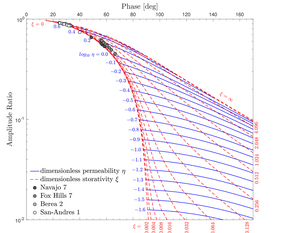

Figure 5: The plot of iso-dimensionless specific storage (dashed red) and iso-dimensionless permeability (solid blue) lines as functions of amplitude ratio and phase lag represents the solutions of Kranz-Bernabé model (reproduced after Bernabé et al. (2006)). Representative data for each sample are plotted for 0.1 Hz oscillation frequency and effective pressures of 3.5 – 62 MPa.

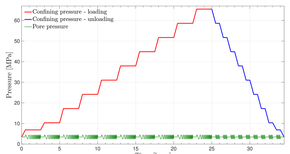

Figure 6: Experimental pressure protocol. Note that the experiment is performed at multiple pore pressure oscillation frequencies during the loading effective pressure path (red curve). The measurements during the unloading path (blue) are done at a single frequency of 0.1 Hz.

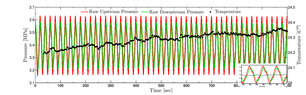

Figure 7: Raw upstream and downstream pore pressures overlain with temperature. The temperature data have been smoothed over a 20 second time interval and indicate temperature variation less than 0.2 °C. The data is shown for the Navajo 7 sample at 62 MPa effective pressure and 0.05 Hz oscillation frequency.

- The experiment is run at various oscillation frequencies (< 1Hz) and confining pressures.
- Raw data (pressures and strains) are acquired and subsequently filtered.
- Hydraulic properties are calculated from pressure amplitude ratio and phase lag, K_{bp} is estimated from strain records.

EXPERIMENTAL RESULTS – HYDRAULIC PROPERTIES

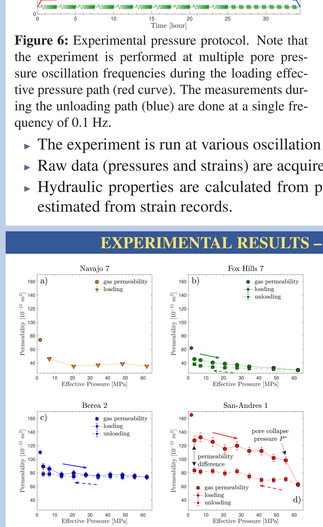

Figure 8: Measured values of permeability as a function of effective pressure at 0.1 Hz oscillation frequency during loading and unloading stress paths for samples Navajo 7 (a), Fox Hills 7 (b), Berea 2 (c), and San-Andres 1 (d). Note the greatest amount of permeability difference in the San-Andres 1 sample.

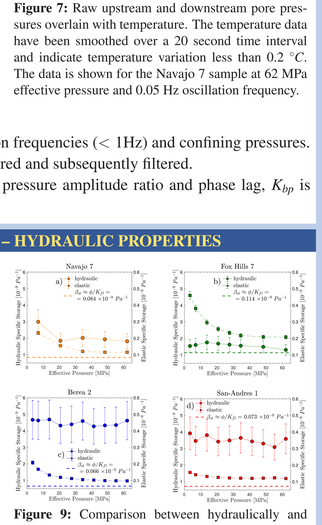

Figure 9: Comparison between hydraulically and elastically derived storage capacities β_{st}, measured at 0.1 Hz oscillation frequency as a function of increasing effective pressure for samples Navajo 7 (a), Fox Hills 7 (b), Berea 2 (c), and San-Andres 1 (d). Dashed line represents the lowest limit of storage capacity, approximated as $\beta_{st} \approx \frac{\phi}{K_{fl}}$.

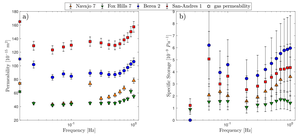

Figure 10: (a) Measured permeability and (b) specific storage as a function of oscillation frequency. The displayed data were measured at an effective pressure of 6.9 MPa. Steady-state gas permeabilities were measured at 1.5 MPa effective pressure.

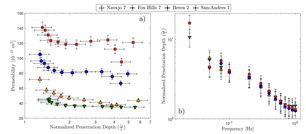

Figure 11: (a) Permeability as a function of the penetration depth, normalized by the sample's length. (b) Penetration depths of the diffusive pore pressure oscillations normalized by the individual sample lengths and plotted as a function of frequencies.

EXPERIMENTAL RESULTS – POROELASTIC PROPERTIES

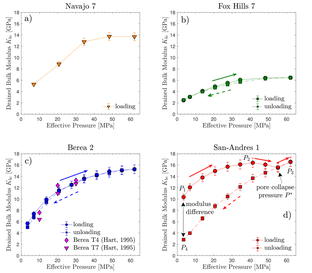

Figure 12: The drained bulk modulus K_{bc} as a function of loading and unloading pressure paths, measured at 0.1 Hz oscillation frequency for samples Navajo 7 (a), Fox Hills 7 (b), Berea 2 (c), and San-Andres 1 (d).

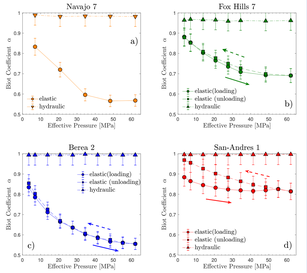

Figure 13: Biot coefficient α as a function of loading and unloading effective pressure for samples Navajo 7 (a), Fox Hills 7 (b), Berea 2 (c), and San-Andres 1 (d). Hydraulically derived Biot coefficients are marked by triangles and are highly-overestimated.

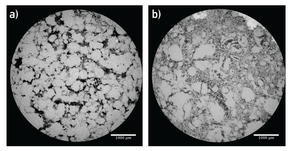

Figure 14: μCT-scans of the San-Andres 1 sample, before and after the hydrostatic loading. Post-experiment μCT image reveals significant pore collapse and grain crushing. (a) The San-Andres 1 sample, before experiment. (b) The San-Andres 1 sample, after experiment.

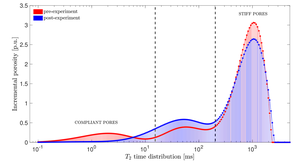

Figure 15: NMR T2 distribution obtained on the post-experiment San-Andres 1 sample (blue curve) shows a significant reduction in amplitude as compared to the pre-experimental measurement (red curve). The NMR data confirm the observation of pore collapse and grain crushing.

NUMERICAL SIMULATIONS

Figure 16: An example of a simulation result for Berea sandstone from Kranz et al. (1990) is shown as series of time-lapse pictures. Pore pressure is plotted with the Darcy velocity field (black arrows) for an upstream pressure oscillation of 1 Hz frequency at a) the beginning of a pressure cycle; b) quarter of the cycle; c) half of the cycle; d) three-quarters of the cycle; e) the end of the cycle. f) One cycle of the upstream pore pressure oscillation, illustrating the time of the simulation snapshots (red circles).

Figure 17: Pressure oscillations extracted at the end of the simulation of Berea sandstone sample from Kranz et al. (1990). Blue curve is the upstream pressure, red is the downstream pressure. Early-time pressure transients vanish after 3-5 cycles. Note the difference in x-axis scales.

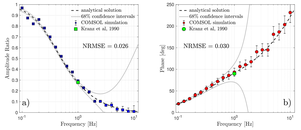

Figure 18: Simulation results for the Berea sandstone sample from Kranz et al. (1990) compared with a forward model and the experimental measurement. a) Amplitude ratio as a function of oscillation frequency. b) Phase as a function of oscillation frequency.

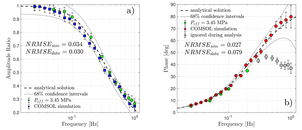

Figure 19: Simulation results for the San-Andres 1 dolostone sample compared with a forward model and the experimental measurements. a) Amplitude ratio as a function of oscillation frequency. b) Phase as a function of oscillation frequency.

INVERSION FOR PERMEABILITY

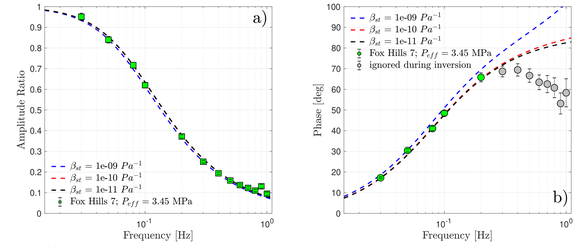

Figure 20: a) Modeled amplitude ratio and b) modeled phase as a function of oscillation frequency for Fox Hills 7 sample at 3.45 MPa effective pressure and plotted with the experimental data. The curves are simulated for a range of storage capacities and permeability of 5.75×10^{-14} m^2.

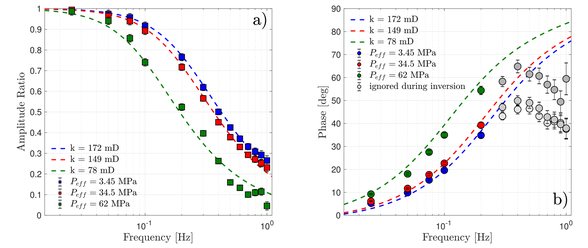

Figure 21: a) Amplitude ratio and b) phase as a function of oscillation frequency for the San-Andres 1 sample, calculated at a range of effective pressures. Gray datapoints are the phases measured at frequencies higher than 0.2 Hz cut-off frequency.

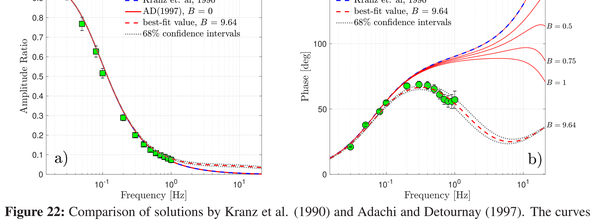

Figure 22: Comparison of solutions by Kranz et al. (1990) and Adachi and Detournay (1997). The curves are simulated for the Fox Hills 7 sample, measured at 34.47 MPa effective pressure. A&D solution is computed for a range of B values. a) Amplitude ratio as a function of oscillation frequency. b) Phase as a function of frequency.

- We use non-linear regression algorithm to calculate the best-fit permeability value for the frequency-dependent amplitude ratio and phase data.
- Due to large downstream reservoir the experiment is insensitive to sample's storage capacity (Figure 20), thus we solve only for permeability.

CONCLUSIONS

- Pore pressure oscillation technique tends to overestimate storage capacities, and as a result, poroelastic coefficients. We use strain gauges to directly measure strains caused by pore pressure pulses, and thus, derive drained bulk modulus and the rest of poroelastic parameters.
- Pore collapse and grain crushing of San-Andres 1 sample has been simultaneously observed in both hydraulic and poroelastic strain measurements, confirming the validity of the method.
- We introduced a novel method for computing permeability from the measured frequency-dependent amplitude ratio and phase datasets. This method is useful for simultaneous determination of permeability and storage capacity from oscillating pore pressure data.

DEDICATION

This poster is dedicated to the loving memory of Dr. Michael L. Batzle.